ChemistrySelect

Research Article
doi.org/10.1002/slct.202500598

Chemistry Europe
European Chemical Societies Publishing

www.chemistryselect.org

ZnO Nanoparticles Synthesized by the Solution Combustion Method for Supercapacitor Applications

Vikas Kumar Pandey,[a] Avaneesh Kumar,[a] Sanjeev Verma,[b] Tapas Das,[c] Saurabh Kumar Pandey,[a] and Bhawna Verma*[a]

Pseudocapacitive materials have demonstrated their transcendence in the recent past. In this manuscript, the authors report the synthesis of ZnO nanoparticles using the solution-combustion method at varying fuel (glycine) compositions for supercapacitor applications. The material characterizations such as XRD, FTIR, SEM, EDX, TEM, XPS, and BET confirmed the successful synthesis of the material. A detailed electrochemical analysis in terms of CD and EIS was conducted. The equal molar ratio (1:1) of zinc nitrate hexahydrate and glycine fuel for ZnO resulted in the highest value of specific capacitance at 98.61 F/g (1 A g^{-1}) under a symmetric 2E configuration in aqueous 1 M KOH electrolyte. The nanoparticles also showed the highest energy density of 13.69 Wh kg^{-1} and 64.10% capacitance retention after 5000 charge-discharge cycles with a minimal charge transfer resistance of 2.37 Ω. The excellent electrochemical behavior of optimized ZnO particles compared to others, was mainly due to the high electrochemically active sites.

1. Introduction

Emissions have caused continuous environmental damage in recent years, despite a decline in the availability of fossil fuels, therefore, developing high-power density and high-energy density-based energy conversion and storage systems is the need of the hour.[1–4] Currently, e-mobility has encouraged many suppliers to use Li-ion batteries because they provide a lot more benefits than they cost. The debate about longevity and performance is still very heated. These gadgets have a higher energy density than conventional capacitors.[5–9] However, the low power density mandates the utilization of new storage technologies to suit the demands. Supercapacitors are extremely promising considering their ability to provide higher energy and power densities than other traditional technologies.[10–13] Based on their charge storage mechanisms, supercapacitors are frequently categorized as electrical double-layer capacitors (EDLCs), pseudocapacitors, and hybrids.[14–17] Additionally, supercapacitors may be recharged in a matter of seconds, unlike batteries, which depend on internal chemical reactions and quickly degrade over time.[18–20] Pseudocapacitors possess better specific capacitance values and energy density than EDLC-based materials because they rely on quick and reversible Faradaic redox processes on the electrode surfaces.[21–24] Recent studies on conducting polymers and oxide-based semiconductors as potential sources of pseudocapacitors have attracted a lot of attention.[25–27] Metal oxides have been extensively studied for usage in supercapacitor applications due to enhanced electrochemical properties such as strong proton conductivity and an extraordinarily reversible redox reaction along with stability. Efficient charge storage with low manufacturing and maintenance costs has thus far been a crucial research challenge for energy storage systems. Metal oxides with special properties, such as NiO, MnO_2, Co_3O_4, and Fe_3O_4, are perfect for supercapacitors.[28–31] Due to its numerous distinctive properties, such as a large band gap (3.37 eV), high exciton binding energy at room temperature, and piezoelectricity, zinc oxide (ZnO) has a wide range of applications in electronics, photocatalysts, and sensors. ZnO has lately been suggested as a viable electro-active material for supercapacitors owing simplicity of production, low cost, environmental friendliness, and abundance.[32–36] Amal AlFawaz et al. obtained a gravimetric capacitance value of 209.8 F g^{-1} at 0.25 A g^{-1} from ZnO nanoparticles used as anode material.[36] Another research from S Rai et al. synthesized ZnO/rGO nanohybrids and reported 345 F g^{-1} of capacitance with excellent retention.[37] Shaheen et al. reported a specific capacitance of 165 F g^{-1} from ZnO-Co_3O_4 nanocomposite with an energy density of 4.2 Wh kg^{-1} in an aqueous 3 M KOH electrolyte.[38] Selvakumar et al. fabricated a symmetrical supercapacitor using a ZnO-activated carbon composite and reported a capacitance of 160 F g^{-1} in 0.1 M Na_2SO_4.[39] In another study, Jayachandiran et al. incurred a capacitance value of 312 F g^{-1} from rGO/ZnO nanocomposite much higher than that of pure ZnO (200 F g^{-1}).[40] Irum et al. studied the effect of NiO on organic framework functionalized ZnO nanoparticles and obtained a specific capacitance of 185

[a] V. K. Pandey, A. Kumar, S. K. Pandey, B. Verma
Department of Chemical Engineering & Technology, IIT BHU, Varanasi 221005, India
E-mail: bverma.che@itbhu.ac.in

[b] S. Verma
Department of Chemical Science & Technology, NIT Patna, Patna, Bihar 800005, India

[c] T. Das
Department of Chemical Engineering, NIT Rourkela, Rourkela, Odisha 769008, India

Supporting information for this article is available on the WWW under https://doi.org/10.1002/slct.202500598

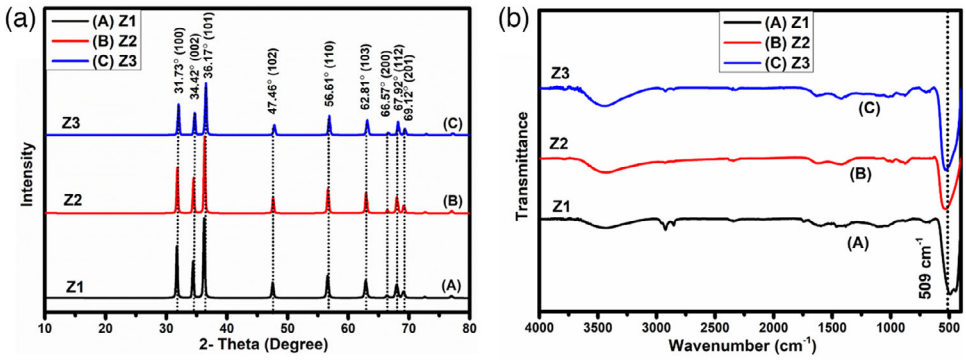

Figure 1. a) XRD, b) FTIR spectrum of different samples.

F/g from the nanocomposite.[23] Saranya et al. synthesized G-ZnO nanocomposite and reported 122 F g^{-1} at 5 mV s^{-1} scan rate.[41] In another research, Shaheen et al. synthesized and reported a semiconducting MoO_3@ZnO nanocomposite that demonstrated ideal capacitive behavior.[42]

In this manuscript, the authors report the effect of glycine fuel on the electrochemical properties of ZnO synthesized from a modified solution-combustion method which is the novelty of this work. This cost-effective glycine-assisted combustion method exploits glycine's dual role as a fuel and a complexing agent to facilitate the synthesis of high-purity, nano-sized ZnO. Glycine acts as a fuel to sustain the combustion process. It reacts with oxidizing agents, such as nitrates (e.g., zinc nitrate), releasing a significant amount of heat. The exothermic nature of the reaction promotes the rapid formation of ZnO with fine particle size. Glycine forms a coordination complex with metal ions, helping to disperse them uniformly before combustion. This ensures homogeneity in the precursor solution and ultimately in the ZnO particles. Charge-discharge (CD) and electrochemical impedance spectroscopy (EIS) study was done in complete detail. Further investigation into admittance and impedance with different input signal frequencies was done using frequency response analysis. Three different samples were prepared and they were physiochemically characterized by XRD (X-ray diffraction), FTIR (Fourier transform infrared spectroscopy), SEM (Scanning electron microscopy), and EDX (Energy-dispersive x-ray analysis).

2. Result and Discussion

2.1. XRD

The XRD spectra for Z1, Z2, and Z3 recorded as bulk material have been provided in Figure 1a. The range of 2-Θ covered was 10–80° and the peaks were seen at the 2-Theta values at 31.73° (100), 34.42° (002), 36.17° (101), 47.46° (102), 56.61° (110), 62.81° (103), 66.57° (200), 67.92° (112), and 69.12° (201). These peaks confirmed the successful synthesis of ZnO (JCPDS 01–79–0206).[43] All the spectroscopic peaks arise at the same location in all three samples Z1, Z2, and Z3, however, a slight difference was seen in terms of peak intensity. This slight difference may be due to the difference in the amount of glycine used to prepare different samples as it may affect the texture and grain size. The crystallinity index for samples Z1, Z2, and Z3 was calculated as 92.09%, 93.18%, and 92.43%, respectively.

2.2. FTIR

The FTIR studies of samples Z1, Z2, and Z3 were conducted to determine the functional groups in the samples. The synthesized materials were combined with KBr and compacted into a pellet for analysis. The FTIR spectra for the samples Z1, Z2, and Z3 have been given in Figure 1b. The spectra were recorded over a wavenumber range of 400 to 4000 cm^{-1}. The absorption band at 509 cm^{-1} was attributed to the presence of ZnO in Z1 sample. The minor peak at 1605 cm^{-1} was attributed to C═C stretching, 1422 to C-H bending. The absorption peak at 2922 cm^{-1} was attributed to CH_2 stretching and bending modes of ZnO.[35] The absorption band present at 2320 cm^{-1} was ascribed to CH_2 deformation.[44] Further, the presence of a wide absorption peak at 3433 cm^{-1} could be ascribed to -OH bending due to some moisture content in the sample. All the absorption bands corresponding to those discussed above were clearly present in the Z2 and Z3 samples Figure 1(b).

2.3. SEM and EDX

The SEM images for the prepared samples Z1, Z2, and Z3 have been displayed in Figure 2. According to morphological analyses, the prepared samples show interconnected particles and agglomerated type of structures. The texture of the powder samples appears to be rough and is responsible for efficient ion transport and reduced resistance. As a result of the constant heating of the precursor, the individually isolated particles are first formed. The presence of roughness on the surface of the zinc oxide nanoparticles enhances the effective surface area for charge accumulation.

Figure 3 depicts all the information in detail on the atomic percentage and weight percentage of each component in the material. The spectrum and the accompanying statistics made it

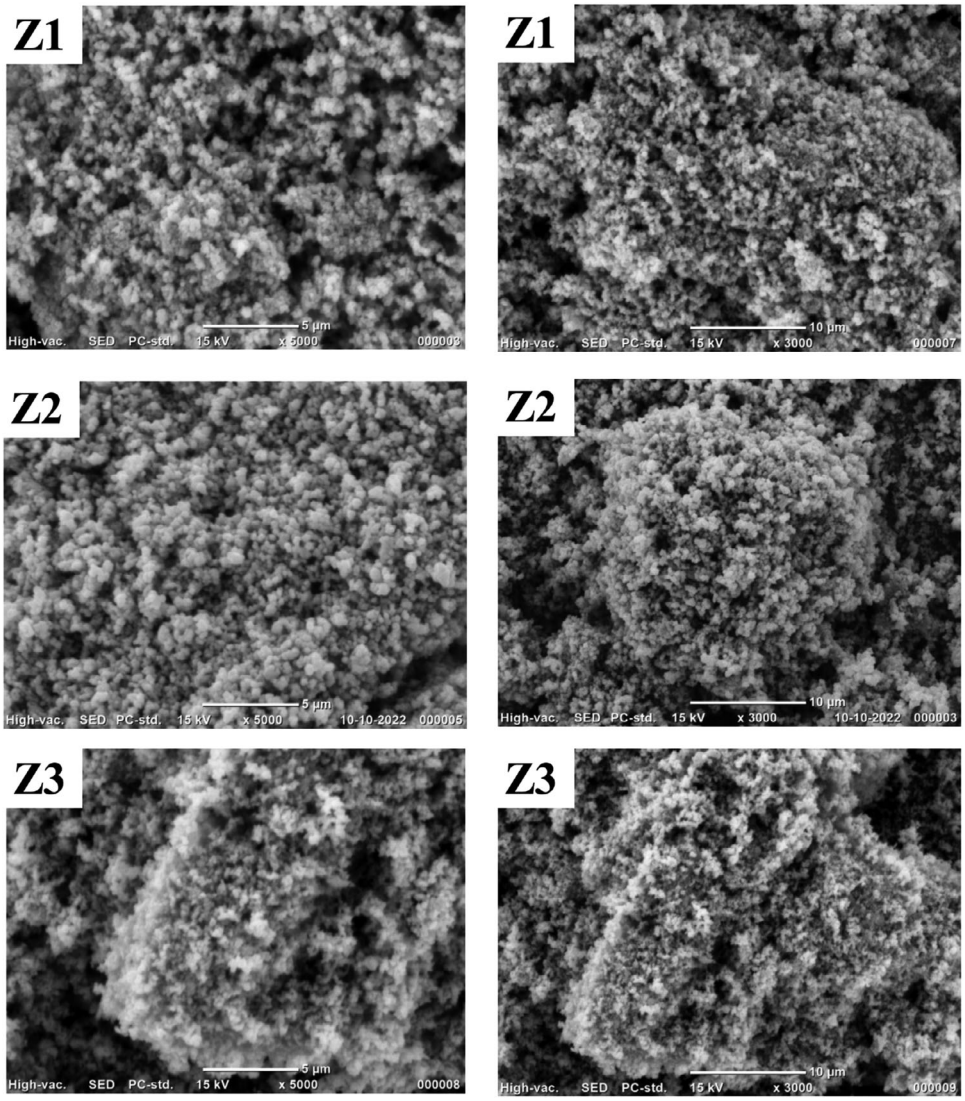

Figure 2. Different SEM images of different samples.

abundantly evident that the ratio of zinc to oxygen is approximately identical to that of the atomic structure.

2.4. TEM, XPS, and BET

The TEM images, XPS studies and BET adsorption-desorption curve of the sample Z2 have been provided in supporting files in Figures S1–S3, respectively. The surface area of Z2 calculated from the BET was found to be 30.26 m^2/g.

2.5. Electrochemical Studies

CD (charge/discharge) curve has been used to assess the electrochemical performance by taking 1 M KOH aqueous electrolytes of the synthesized materials.[45] The CD behavior of several synthetic materials was depicted in Figure 4a using a 2E symmetric system with a constant current density (1 A/g). Z2 material demonstrated longer charge/discharge times than other materials, and it is generally known that Z2 has the highest capacitance values due to its long charge/discharge times (Equation 1).

$$C_s = \frac{I * td}{ma * \Delta V}\ [2E\ CD] \quad (1)$$

C_s (F/g) = Specific capacitance using symmetric 2E; m_a (mg) = Material active mass; I (mA) = Discharging current; t_d (s) = Discharging time; ΔV (Volt) = Stable voltage window

Similar to this, the Z2's charge/discharge times were altered as a function of current density, as shown in Figure 4b, and it was discovered that when current density climbed, charge and discharge times decreased. In this way, the specific capacitance value for Z2 was determined to be lowest at the current density of 50 A g^{-1} and maximum at 1 A g^{-1} of current density. CD plots of Z1 and Z3 at different current densities are also shown in Figure 4c,d. It is possible that the shape of the curves in the CD curve, which are not perfectly triangular (deformed), is a result of the pseudocapacitive components like Zn particles. A very low ohmic drop (IR loss) was found, pointing to the system's excel-

Research Article
doi.org/10.1002/slct.202500598

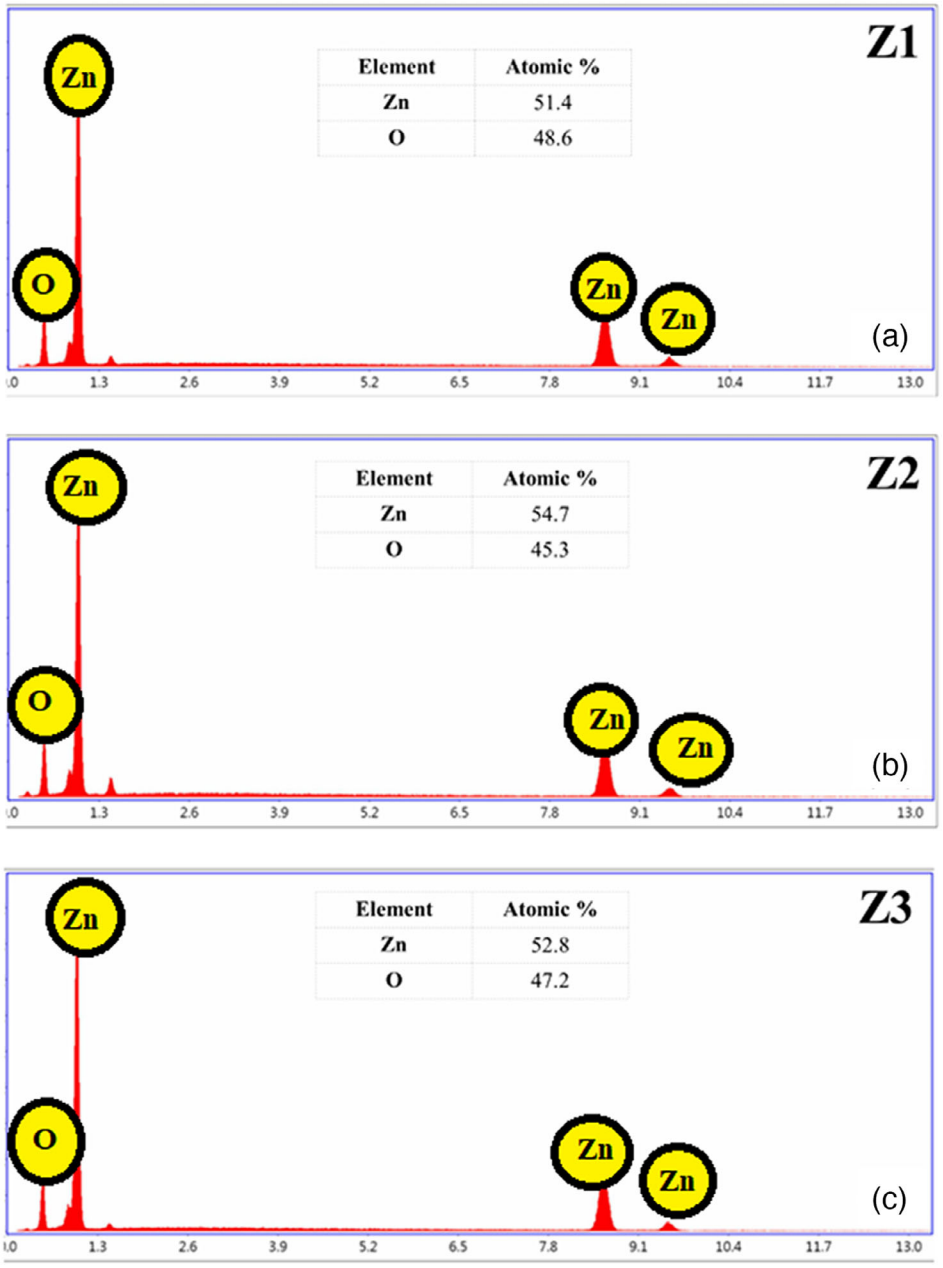

Figure 3. EDX spectrum of different samples, a) Z1, b) Z2 and, c) Z3.

lent reversibility. Using a CD plot, Table 1 presents various specific capacitance values. Low specific capacitance values are obtained because a higher value of current density causes the immobile areas of the electrode active material to create the charge diffusion hurdle. CD plot of Z2 at different CD cycles has also been provided in Figure 4e.

The cyclic voltammetric curves of the synthesized materials Z1, Z2, and Z3 have been presented in Figure S4A for a scan rate value of 5 mV s^{-1}. A typical pseudocapacitive type of behavior was observed for all the materials depicting a well-defined pair of cathodic and anodic peaks. The material Z2 demonstrated the highest voltammetric area under the CV curve followed by Z3 and Z1. The calculated specific capacitance was obtained as 162.3, 189.7, and 175.6 F g^{-1} for Z1, Z2 and Z3, respectively. These results are perfectly in line with the specific capacitance values calculated by charge-discharge curves. Z2 has been the best sample showing the highest specific capacitance and electroactivity. The reason for the same may be the stoichiometric glycine ratio. In the case of lean fuel-based material (Z1), incomplete combustion occurs resulting in poor purity and incomplete decomposition of precursors of the zinc oxide nanoparticles. When using rich fuel as in the case of Z3, excessive heat energy is liberated as a consequence of multiple side reactions thereby trapping the relatively higher amount of residues in the zinc oxide nanoparticles. The use of stoichiometric amounts of fuel utilizes the kinetics of the reaction properly to form a more uniform and higher-purity product. Further, the scan rate values were varied in order to study the behavior of the best material Z2 under such conditions.

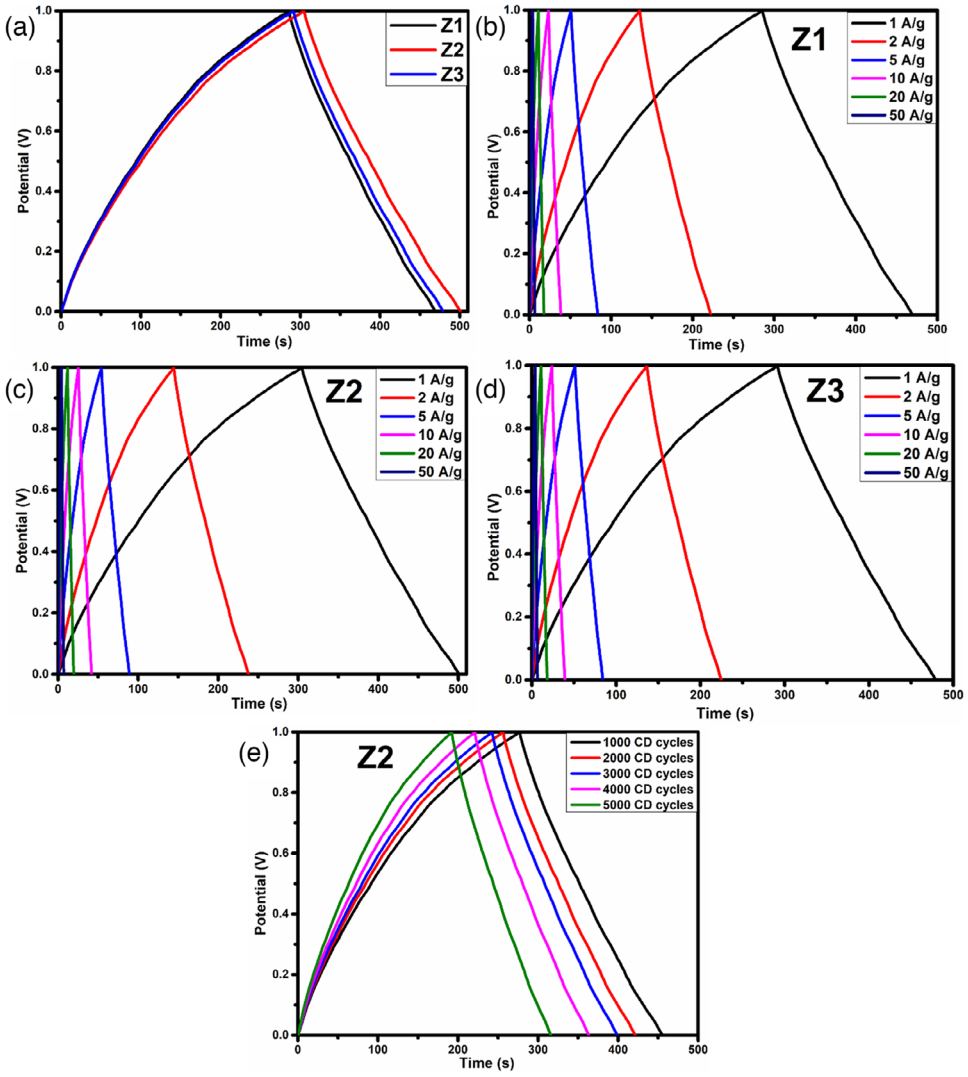

Figure 4. a) CD curve of different samples, b) CD curve of Z1 at different current densities, c) CD curve of Z2 at different current densities, d) CD curve of Z3 at different current densities, e) CD curve of Z2 versus number of cycles.

Table 1. Different specific capacitance, specific energy, and specific power values of different samples.

Current Density [A/g] Or Scan rate [mV/s]	CV 3E C_s (Z1) [F/g]	CV 3E C_s (Z2) [F/g]	CV 3E C_s (Z3) [F/g]	CD 2E C_s (Z1) [F/g]	CD 2E C_s (Z2) [F/g]	CD 2E C_s (Z3) [F/g]	E_{sp} (Z1) [Wh/kg]	E_{sp} (Z2) [Wh/kg]	E_{sp} (Z3) [Wh/kg]	P_{sp} (Z1) [kW/kg]	P_{sp} (Z2) [kW/kg]	P_{sp} (Z3) (kW/kg)
1	–	–	–	92.28	98.61	94.23	12.81	13.69	13.08	0.24	0.25	0.24
2	–	–	–	87.31	93.49	88.36	12.12	12.98	12.26	0.49	0.49	0.49
5	162.3	189.7	175.6	82.10	87.45	82.81	11.40	12.14	11.50	1.24	1.24	1.24
10	–	121.4	–	75.32	82.16	77.10	10.45	11.41	10.70	2.49	2.49	2.48
20	–	74.3	–	69.43	76.47	71.42	9.63	10.62	9.91	4.98	4.99	4.98
50	–	38.5	–	63.61	69.23	66.73	8.83	9.61	9.26	12.48	12.49	12.48

The CV curves for the material Z2 have been presented in Figure S4B. It was observed that, with the rising values of scan rates, the values of peak current significantly increase. Also, the anodic peaks were shifted slightly to the right, and cathodic peaks were shifted slightly to the left with the increase in scan rates indicating the presence of strong polarization and kinetic irreversibility. The specific capacitance values at 10, 20, and 50 mV s^{-1} scan rates were obtained as 121.4, 74.3, and 38.8 F g^{-1} for Z2 as shown in Table 1.

Figure 5a–c shows the change of capacitance with current density employing a 2E system and inferred that the value of particular capacitance declines in the system as the current density

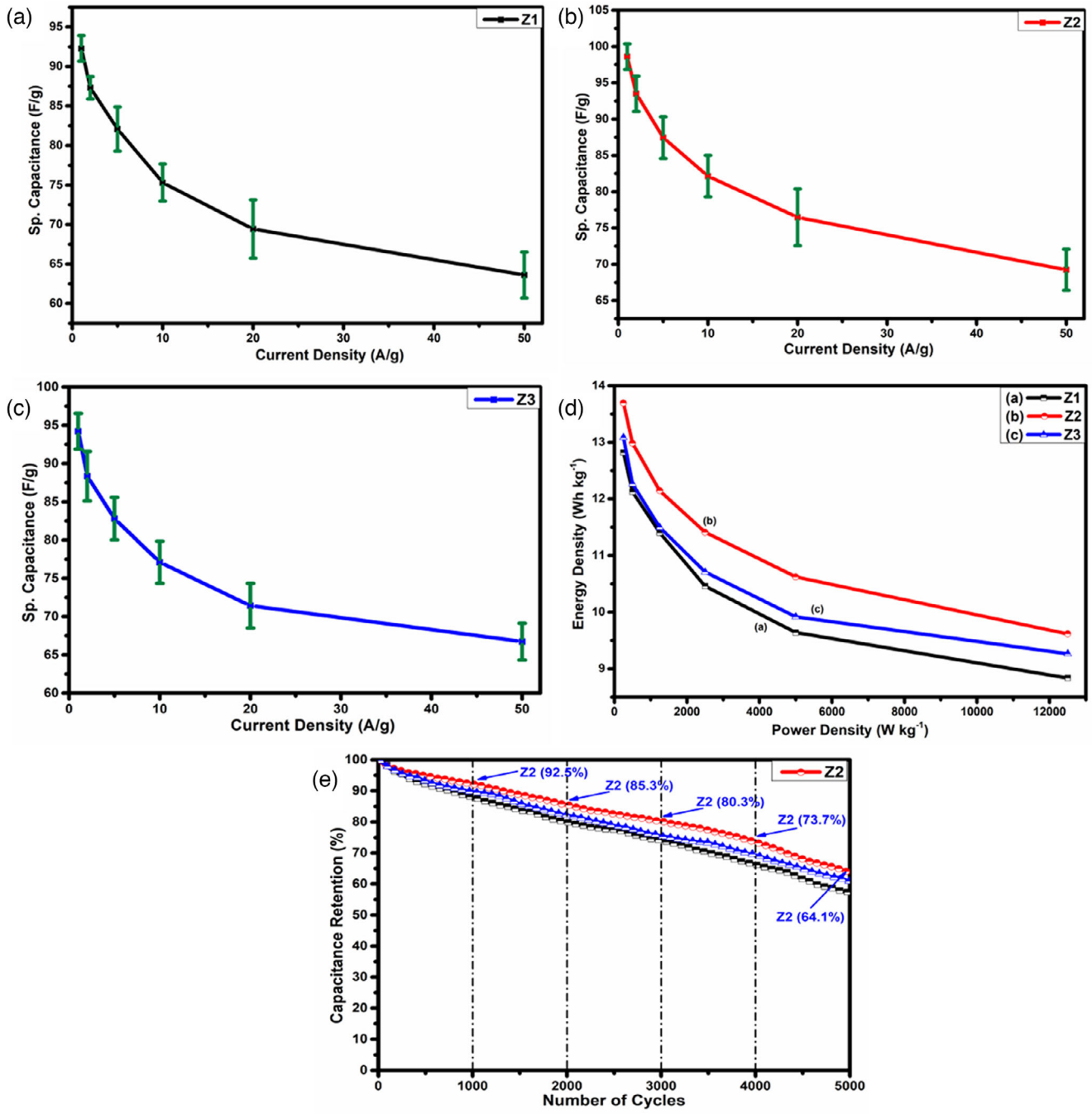

Figure 5. a) Variation of specific capacitance versus current density of Z1 sample, b) Variation of specific capacitance versus current density of Z2 sample, c) Variation of specific capacitance versus current density of Z3 sample d) Ragone plot of different sample, and e) Capacitance retention percentage plot of different sample.

rises. The functioning of supercapacitor material is also governed by two key factors: specific energy (E_{sp}) and specific power (P_{sp}). E_{sp} corresponds to the accumulation of charges, whereas P_{sp} describes the capability to transmit charges.[46] The relevant values were determined using Equations (2) and (3).

$$P_{sp} = \frac{E_{sp}}{t_d} \quad (2)$$

$$E_{sp} = \frac{1}{2} C_s V^2 \quad (3)$$

E_{sp} (Wh/kg) = Specific energy; P_{sp} (W/kg) = Specific power; C_s (F/g) = Symmetric 2E specific capacitance; V (Volt) = Voltage window; t_d (s) = Discharging time

Additionally, Figure 5d Ragone plot shows the change of Psp and Esp for various synthesized materials. In comparison to other prepared materials, the Z2 demonstrated a high specific energy value. Table 1 lists the specific energy and power values for several materials, and it is claimed that Z2 has higher specific energy than the rest. However, the fact that the specific powers of the various samples are nearly identical indicates that all

Table 2. Comparison of specific capacitance, energy density, and power values in contrast with previously reported works.

Sample	Scan Rate [mV/s]/ Current Density [A/g]	Specific Capacitance [F/g]	Sp. Energy Density [Wh/kg]	Sp. Power Density [W/kg]	Ref.
ZnO	0.25 A g^{-1}	209.8	4.66	1145	[36]
ZnO/rGO	5 mV s^{-1}	345	7.66	30.89	[37]
$NiCo_2O_4$/ NCW	1 A g^{-1}	1730	56.1	349	[47]
$ZnCl_2$ treated CF	1 A g^{-1}	105	–	–	[48]
ZnO-Co_3O_4	2 mV s^{-1}	165	4.1	7500	[38]
ZnO/AC	2 mV s^{-1}	160	–	–	[39]
rGO/ZnO	5 mV s^{-1}	312	–	–	[40]
F-doped ZnO	10 mV s^{-1}	12.2	11.2	250	[49]
ZnO/C	50 mV s^{-1}	21.7	–	–	[50]
MnO@CNPs	0.5 A g^{-1}	545	27	176	[51]
N-doped carbon	0.5 A g^{-1}	275	12.6	4980	[52]
Polyimide/cellulose composite	1 A g^{-1}	300	22.6	800	[53]
MnO-carbon	1 A g^{-1}	550	50.2	800	[54]
PCG	1 A g^{-1}	420	31.3	500	[55]
ZnO	5 mV s^{-1} & 1 A g^{-1}	189.7 & 98.61	13.69	2500	**Present work**

NCW- nitrogen carbonized wood, CF- carbon fibers, PCG- nitrogen, sulfur co-doped pollen derived carbon/graphene

materials have the same capability for transmitting the ions that have been accumulated inside themselves. Now that we have obtained the various values of P_{sp} and E_{sp} at different current densities, we have observed that as current density increases, E_{sp} value is continuously reducing, while P_{sp} value is continuously growing. Table 2 demonstrates a comparison of specific capacitance, energy density, and power values in contrast with previously reported works.

Further, the cycling stability of the produced materials was examined up to 5000 CD cycles at 1 A/g current density, and for the Z2, 64.10% capacitive retention was still present after 5000 CD cycles, which was greater than Z1 (57.31% after 5000 cycles) and Z3 (60.43% after 5000 cycles) (Figure 5e). There is less interaction between the electrode and electrolyte, which causes capacitance loss. Z2 has been the best sample showing the highest specific capacitance and best electroactivity. The reason for the same may be the stoichiometric glycine ratio. In the case of lean fuel-based material (Z1), incomplete combustion occurs resulting in poor purity and incomplete decomposition of precursors of the zinc oxide nanoparticles. When using rich fuel as in the case of Z3, excessive heat energy is liberated as a consequence of multiple side reactions thereby trapping the relatively higher amount of residues in the zinc oxide nanoparticles. The use of stoichiometric amounts of fuel utilizes the kinetics of the reaction properly to form a more uniform and higher-purity product.

EIS was used in 1 M KOH aqueous electrolyte to evaluate the various resistances such as charge-transfer resistance (R_{ct}), equivalent series or bulk resistance (R_s), resistance due to capacitive behavior, and Warburg impedance/diffusion resistance (w) of the synthesized material (Figure 6a).[56] This analysis was done to determine the electrochemical action of the prepared materials on the interface. The R_{ct} value is defined as plotted semicircle diameter, and the intercept toward the origin in the x-axis is defined as R_s. The combined resistance of the material and the electrolyte solution is the main cause of R_s. The R_s values for Z1, Z2, and Z3 are 2.32, 1.33, and 1.52 Ω, respectively. The very identical ionic resistance of the medium, but a lower R_s value for Z2 because of their reduced intrinsic resistance. Similar to this, the R_{ct} values for Z1, Z2, and Z3 are determined to be 4.62, 2.37, and 6.37 Ω respectively. R_{ct}'s lowering order made mention of the improved electronic conductivity. The fact that Z2 has the smallest R_{ct} value of all, may be related to the material's higher number of active sites and its ease of ion transport. The superior electrode/electrolyte contact and the significant amount of active sites in Z2 contribute to the smooth ion diffusion and the favorable ion penetration on the surface of Z2. Also, the equivalent electrical circuit of Z2 has been given in Figure 6a. In essence, different types of resistance including EDLC, pseudo, and constant phase elements (Q), are present. The parameter explaining the supercapacitor's non-ideality is known as the constant phase element (Q). The diffusion mechanism of electrolytes in electrodes involves a combination of ion movement through the electrolyte, intercalation into the electrode, and diffusion within the electrode material itself. The efficiency of this process is influenced by the electrode structure, electrolyte properties, temperature, and electrochemical conditions.

To assess the responses (T_r) of various samples, Figure 6b shows the changes in admittance between both the real and imaginary directions. From the responsiveness (T_r) given by Equation (4), it is possible to determine the system's willingness during the electrochemical reactions.

$$T_r = \frac{1}{F_k} \tag{4}$$

The knee frequency can be used to gather data regarding the use of charges that are collected in a system. The responsiveness

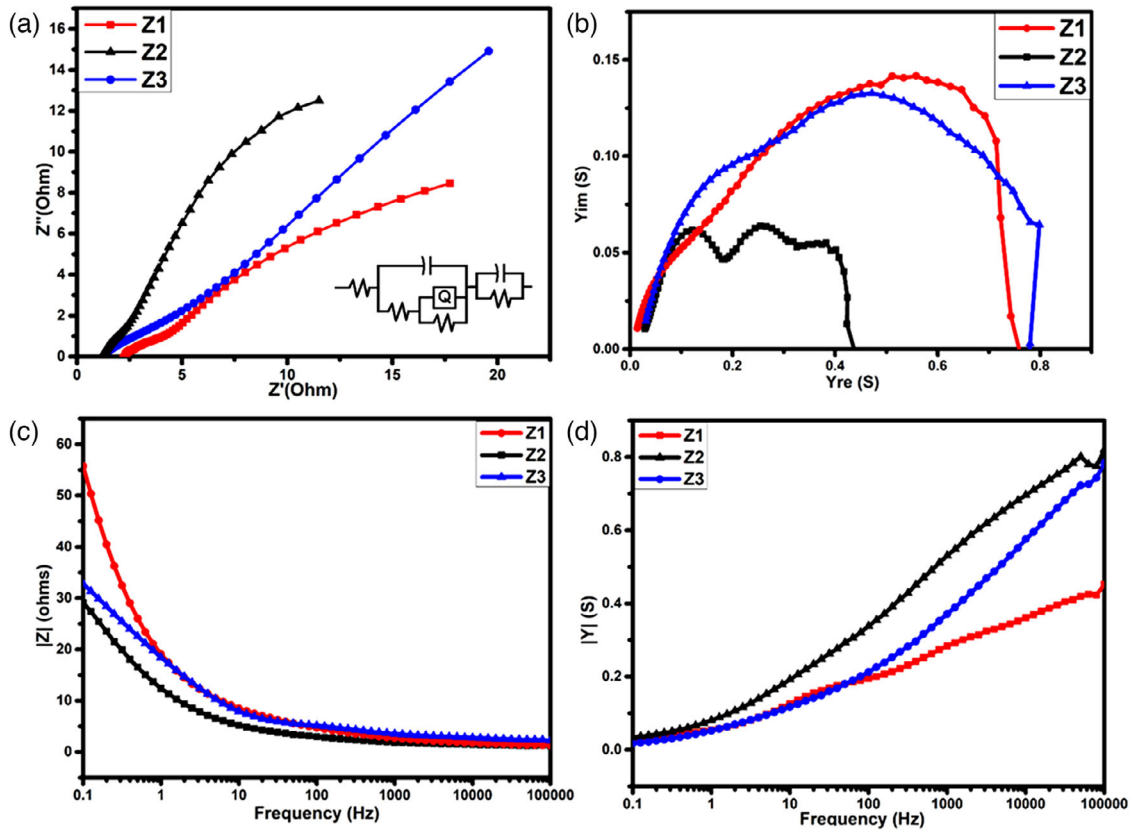

Figure 6. a) EIS plot of different samples, b) Yim versus Yre plot of different samples, c) Impedance (|Z|) spectra of different samples, d) Admittance (|Y|) spectra of different samples.

Table 3. Knee frequency and response time values of different samples.

Sample	F_k [Hz]	T_r [ms]
Z1	25.11	39.82
Z2	63.09	15.85
Z3	39.81	25.11

(T_r) and knee frequency (F_k) of several samples are displayed differently in Table 3. Z2 has a low response time due to fast pseudo-actions in the electrode/electrolyte interface.

The impedance (|Z|) spectra for Z1, Z2, and Z3 are displayed in Figure 6c, sequentially. It is clear that the total impedance (|Z|), is greater at low frequencies and lower at high frequencies. With a rise in frequency, the total impedance value |Z| falls. At low frequency, the |Z| for Z2 seems to be the minimum and largest for Z1. This reflects the small resistance in Z2 and the high resistance in Z1. The outcomes of the Nyquist plot already proved that Z2 seemed to have the smallest R_{ct} value.

The admittance (|Y|) spectra of several samples are also shown in Figure 6d. According to the plot, the |Y| value rises from low to extremely high frequency. Inversion of impedance is the only thing admittance |Y|. Z2 exhibits the largest |Y| value at a lower frequency compared to other materials, which may be a result of Z2's strong conductivity. Superior admittance of all the synthesized samples may be mostly due to the quicker ions' passage across the electrode surface. The electrical equivalent circuit of different materials has been given in Figure S1A–C. In essence, a variety of resistances, including constant phase elements (Q), and pseudo, are present. The parameter that best describes the nonideality of the supercapacitor is the constant phase element (Q).

3. Conclusion

In conclusion, Z2 (1:1) was prepared successfully and demonstrated improved electrochemical behavior as a supercapacitor material compared to other materials. The Z2 showed a high C_s of 98.61 F g^{-1} at 1 A g^{-1}, using a symmetric 2E system. The Z2 also illustrated higher E_{sp} of 13.69 Wh kg^{-1}, 12.49 kW kg^{-1} P_{sp}, and cyclic stability of 64.10% up to 5000 CD cycles with a low R_{ct} of 2.37 Ω. Because of its high E_{sp} and extended cycle stability, Z2 is a promising contender for supercapacitor electrode material with other carbon-based materials.

4. Experimental Section

For material synthesis, zinc nitrate hexahydrate[$Zn(NO_3)_2.6\ H_2O$] and glycine (amino acetic acid – $C_2H_5NO_2$) were procured from Sigma Aldrich for the preparation of ZnO particles. Initially, 0.1 mol of zinc nitrate hexahydrate was dissolved in 150 ml of double-distilled water and stirred continuously for 30 min. Subsequently, 0.05 mol

of glycine was added to the solution and stirred for an additional hour. The mixture was then heated to 80 °C to initiate sol-gel formation. The resulting sol-gel was transferred to a hot plate maintained at the same temperature. Zinc oxide (ZnO) particles were formed upon the release of fumes and combustion. These particles were calcined in a muffle furnace at 700 °C and ground into a fine powder, designated as sample Z1. Two additional samples, Z2 and Z3, were prepared using zinc nitrate hexahydrate and glycine in molar ratios of 1:1 and 1:1.5, respectively. Fine grinding is essential to achieve a homogenous powder as bulk material. Once the sample is prepared, it should be evenly spread on a flat holder, such as a sample slide or holder, ensuring a smooth surface to minimize scattering errors.

For electrode preparation, the electroactive material slurry was prepared by mixing isopropanol, Nafion solution, and active material. The active material slurry was applied on Nickel foam ($1 \times 1\ cm^2$) to get the active material loading of ≈2.5 mg and dried subsequently in the oven for 4 hours. The same material for the positive and negative electrodes was used for a symmetric two-electrode system. Whatman GF/F filter paper was used as a separator with 1 M KOH electrolyte to divide these two symmetric electrodes.

The crystallographic behavior of all the synthesized samples was identified by X-ray diffractometer Miniflex 600 (Rigaku Corporation) by using Cu k-alpha radiation (1.54 Å) between 10°–80° of 2θ range at a scan rate of 4°/min as bulk material. Cu Kα radiation ($\lambda = 1.5406$ Å) is used. The angular range (2θ) was from 10° to 80°. The existence of various functional groups was confirmed by the FTIR spectrometer (Nicolet iS5 Thermo scientific FTIR spectrometer LLC) in between 4000 and 400 cm^{-1} wavenumber. The morphological analysis was performed by using EVO- Scanning Electron Microscope MA 15/18 of Zeiss Microscopy Ltd. The EDX analysis was performed with the help of 51N1000 – EDS System of Oxford Instruments Nanolysis. The TEM studies were performed at Tecnai G2 20 Twin from FEI USA. The XPS analysis was conducted using the K-alpha model of Thermo Fisher Scientific.

Author Contributions

V.K.P. performed conceptualization, methodology, and writing the original draft. A.K. performed visualization, investigation, editing, and reviewing. S.V. performed visualization, editing, and reviewing. T.D. performed investigation, editing, and reviewing. S.K.P. performed visualization and investigation. B.V. performed supervision, conceptualization, reviewing, and editing.

Acknowledgements

The authors are highly grateful to the Ministry of Human Resource Development, India (MHRD, India) and the Indian Institute of Technology BHU, Varanasi for providing hassle-free lab facilities to carry out the required research work.

Conflict of Interests

The authors declare no conflict of interest.

Data Availability Statement

Data available on request from authors.

Keywords: Charge-discharge · Electrochemical impedance spectroscopy · Energy storage · Supercapacitor · Zinc oxide nanoparticles

[1] T. Xing, Y. Ouyang, Y. Chen, L. Zheng, C. Wu, X. Wang, *J. Energy Storage* **2020**, *28*, 101248.
[2] L. Wang, Y. Li, M. Xia, Z. Li, Z. Chen, Z. Ma, X. Qin, G. Shao, *J. Power Sources* **2017**, *347*, 220–228.
[3] M. Zhang, Y. Li, Z. Shen, *J. Power Sources* **2019**, *414*, 479–485.
[4] S. Verma, B. Verma, *Bioresour. Technol. Reports* **2023**, *21*, 101354.
[5] P. Lamba, P. Singh, P. Singh, P. Singh, Bharti, A. K., M. Gupta, Y. Kumar, *J. Energy Storage* **2022**, *48*, 103871.
[6] W. Huang, L. Li, D. Liang, W. Zhou, H. Wang, Z. Lu, S. Yu, Y. Fan, *Inorg. Chem. Front.* **2019**, *6*, 2927–2934.
[7] L. Li, J. Meng, M. Zhang, T. Liu, C. Zhang, *Chem. Commun.* **2022**, *58*, 185–207.
[8] S. Cheng, Z. Dai, J. Fu, P. Cui, K. Wei, Y. Zhang, Y. Wu, Y. Liu, Z. Sun, Z. Shao, X. Cui, Q. Su, E. Xie, *J. Mater. Chem. A.* **2021**, *9*, 622–631.
[9] F. Naseri, S. Karimi, E. Farjah, E. Schaltz, *Renew. Sustain. Energy Rev.* **2022**, *155*, 111913.
[10] I. Shaheen, K. S. Ahmad, *Mater. Innov.* **2022**, *2*, 255-268.
[11] P. Xu, Q. Yuan, W. Ji, Y. Zhao, R. Yu, Y. Su, N. Huo, *Crystals* **2023**, *13*, 282.
[12] Y. Zhao, *J. Mater. Res. Technol.* **2022**, *21*, 546–560.
[13] H. Yu, Y. Chen, W. Wei, X. Ji, L. Chen, *ACS Nano* **2022**, *16*, 9736–9747.
[14] T. Das, S. Verma, V. K. Pandey, B. Verma, Polymer-Based Electrolytes, **2023**, pp. 33–47, https://doi.org/10.1007/978-981-99-4193-3_3.
[15] S. Verma, B. Verma, *J. Ind. Eng. Chem.* **2024**, *140*, 354-363.
[16] X. Han, G. Xiao, Y. Wang, X. Chen, G. Duan, Y. Wu, X. Gong, H. Wang, *J. Mater. Chem. A.* **2020**, *8*, 23059–23095.
[17] Y. He, F. Wang, G. Du, L. Pan, K. Wang, R. Gerhard, R. Plath, P. Rozga, P. Trnka, *High Volt.* **2023** *8* 305–314.
[18] J. Xiao, H. Li, H. Zhang, S. He, Q. Zhang, K. Liu, S. Jiang, G. Duan, K. Zhang, *J. Bioresour. Bioprod.* **2022**, *7*, 245–269.
[19] Y. Wang, L. Zhang, H. Hou, W. Xu, G. Duan, S. He, K. Liu, S. Jiang, *J. Mater. Sci.* **2021**, *56*, 173–200.
[20] S. Verma, B. Verma, *Colloids Surfaces A Physicochem. Eng. Asp.* **2023**, *682*, 132893.
[21] J. Liu, D. Xuan, Z. Lu, Z. Wang, Q. Liu, S. Li, D. Wang, Y. Ye, D. Wang, Z. Zheng, *Appl. Surf. Sci.* **2022**, *573*, 151626.
[22] V. K. Pandey, S. Verma, T. Das, B. Verma, *Bioresour. Technol. Reports* **2022**, *20*, 101255.
[23] I. Shaheen, K. S. Ahmad, C. Zequine, R. K. Gupta, A. G. Thomas, M. A. Malik, *Int. J. Energy Res.* **2020**, *44*, 5259–5271.
[24] S. Verma, S. Verma, S. Kumar, B. Verma, *Nanowires*, CRC Press, Boca Raton **2023**, pp. 135–148.
[25] S. N. Amirtharaj, M. Mariappan, *Appl. Phys. A.* **2021**, *127*, 607.
[26] W. Su, R. Miao, B. Tao, F. Miao, *Ionics* **2019**, *25*, 5419–5427.
[27] T. Das, S. Verma, V. K. Pandey, B. Verma, in *Nanowires*, CRC Press, Boca Raton **2023**, pp. 269–282.
[28] N. Mohammadi, K. Pourreza, N. Bahrami Adeh, M. Omidvar, *J. Alloys Compd.* **2021**, *883*, 160874.
[29] L. Li, R. Xiao, X. Tao, Y. Wu, L. Jiang, Z. Zhang, Y. Qing, *J. Power Sources* **2021**, *491*, 229618.
[30] S. Verma, V. K. Pandey, B. Verma, *Mater. Technol.* **2022**, 1–17.
[31] S. Verma, V. K. Pandey, R. K. Gupta, S. Verma, B. Verma, *Pseudocapacitors*, Springer **2024**, pp. 375–387, https://doi.org/10.1007/978-3-031-45430-1_20.
[32] S. Heydari, A. Asefnejad, N. Hassanzadeh Nemati, V. Goodarzi, A. Vaziri, *React. Funct. Polym.* **2022**, *170*, 105126.
[33] P. Tayebi, A. Asefnejad, H. A. Khonakdar, *Polym. Technol. Mater.* **2021** 1–16.
[34] Z. Guo, R. Zhan, Y. Shi, D. Zhu, J. Pan, C. Yang, Y. Wang, J. Wang, *Chem. Eng. J.* **2023**, *456*, 141157.
[35] S. R. Yekkaluri, S. Konda, D. Velpula, R. K. Thida, S. C. Chidurala, B. N. Tumma, N. R. Nama, R. Deshmukh, *Appl. Surf. Sci. Adv.* **2022**, *12*, 100326.
[36] A. AlFawaz, A. Ahmad, N. Ahmad, F. A. Alharthi, *Phys. Scr.* **2022**, *97*, 030009.
[37] S. Rai, R. Bhujel, M. Khadka, R. L. Chetry, B. P. Swain, J. Biswas, *Mater. Today Chem.* **2021**, *20*, 100472.
[38] I. Shaheen, K. S. Ahmad, C. Zequine, R. K. Gupta, A. G. Thomas, M. A. Malik, *New J. Chem.* **2020**, *44*, 18281–18292.

[39] M. Selvakumar, D. Krishna Bhat, A. Manish Aggarwal, S. Prahladh Iyer, G. Sravani, *Phys. B Condens. Matter.* **2010**, *405*, 2286–2289.
[40] J. Jayachandiran, J. Yesuraj, M. Arivanandhan, A. Raja, S. A. Suthanthiraraj, R. Jayavel, D. Nedumaran, *J. Inorg. Organomet. Polym. Mater.* **2018**, *28*, 2046–2055.
[41] M. Saranya, R. Ramachandran, F. Wang, *J. Sci. Adv. Mater. Devices* **2016**, *1*, 454–460.
[42] I. Shaheen, K. S. Ahmad, S. B. Jaffri, D. Ali, *Renew. Energy* **2021**, *167*, 568–579.
[43] S. Talam, S. R. Karumuri, N. Gunnam, *ISRN Nanotechnol.* **2012**, *2012*, 1–6.
[44] K. Sreekanth, T. Siddaiah, N. O. Gopal, Y. M. Kumar, C. Ramu, *J. Sci. Adv. Mater. Devices* **2019**, *4*, 230–236.
[45] T. Das, B. Verma, *Synth. Met.* **2019**, *251*, 65–74.
[46] S. Verma, B. Verma, *Nanostructured Materials for Supercapacitors*, Springer **2022**, pp. 221–244, https://doi.org/10.1007/978-3-030-99302-3_11.
[47] J. Yang, H. Li, S. He, H. Du, K. Liu, C. Zhang, S. Jiang, *Polymers* **2022**, *14*, 2521.
[48] G. Duan, L. Zhao, L. Chen, F. Wang, S. He, S. Jiang, Q. Zhang, *New J. Chem.* **2021**, *45*, 22602–22609.
[49] F. Erdemir, E. Tuzcu, S. Bilgin, Ü. Alver, A. Çanakçı, *Mater. Chem. Phys.* **2021**, *259*, 124033.
[50] M. Jayalakshmi, M. Palaniappa, K. Balasubramanian, *Int. J. Electrochem. Sci.* **2008**, *3*, 96–103.
[51] W. Guo, X. Guo, L. Yang, T. Wang, M. Zhang, G. Duan, X. Liu, Y. Li, *Polymer* **2021**, *235*, 124276.
[52] F. Wang, L. Chen, H. Li, G. Duan, S. He, L. Zhang, G. Zhang, Z. Zhou, S. Jiang, *Chinese Chem. Lett.* **2020**, *31*, 1986–1990.
[53] H. Li, L. Cao, H. Zhang, Z. Tian, Q. Zhang, F. Yang, H. Yang, S. He, S. Jiang, *J. Colloid Interface Sci.* **2022**, *609*, 179–187.
[54] Z. Tian, H. Li, W. Yang, S. Jian, C. Zhang, S. Jiang, *Diam. Relat. Mater.* **2023**, *131*, 109582.
[55] L. Cao, H. Li, X. Liu, S. Liu, L. Zhang, W. Xu, H. Yang, H. Hou, S. He, Y. Zhao, S. Jiang, *J. Colloid Interface Sci.* **2021**, *599*, 443–452.
[56] S. Verma, T. Das, S. Verma, V. K. Pandey, S. K. Pandey, H. Verma, B. Verma, *Fuel* **2025**, *381*, 133517.

Manuscript received: January 30, 2025